NeuroMolecular Medicine (2019) 21:303–313
https://doi.org/10.1007/s12017-019-08551-9

ORIGINAL PAPER

eIF2B Mutations Cause Mitochondrial Malfunction in Oligodendrocytes

Melisa Herrero[1] · Shir Mandelboum[2] · Orna Elroy-Stein[1,2]

Received: 22 April 2019 / Accepted: 20 May 2019 / Published online: 27 May 2019

Abstract
Vanishing white matter (VWM) disease (OMIM#306896) is an autosomal recessive neurodegenerative leukodystrophy caused by hypomorphic mutations in any of the five genes encoding the subunits of eukaryotic translation initiation factor 2B (eIF2B). The disease is manifested by loss of cerebral white matter and progressive deterioration upon exposure to environmental and physiological stressors. "Foamy" oligodendrocytes (OLG), increased numbers of oligodendrocytes precursor cells (OPC), and immature defective astrocytes are major neuropathological denominators. Our recent work using Eif2b5$^{R132H/R132H}$ mice uncovered a fundamental link between eIF2B and mitochondrial function. A decrease in oxidative phosphorylation capacity was observed in mutant astrocytes and fibroblasts. While an adaptive increase in mitochondria abundance corrects the phenotype of mutant fibroblasts, it is not sufficient to compensate for the high-energy demand of astrocytes, explaining their involvement in the disease. To date, astrocytes are marked as central for the disease while eIF2B-mutant OLG are currently assumed to lack a cellular phenotype on their own. Here we show a reduced capacity of eIF2B-mutant OPC isolated from Eif2b5$^{R132H/R132H}$ mice to conduct oxidative respiration despite the adaptive increase in their mitochondrial abundance. We also show their impaired ability to efficiently complete critical differentiation steps towards mature OLG. The concept that defective differentiation of eIF2B-mutant OPC could be a consequence of mitochondrial malfunction is in agreement with numerous studies indicating high dependency of differentiating OLG on accurate mitochondrial performance and ATP availability.

Keywords Leukodystrophy · EIF2B · Vanishing white matter disease · Translation · Oxidative phosphorylation · Oligodendrocyte differentiation

Introduction

Mutations in any of the genes encoding the five subunits of eukaryotic translation initiation factor 2B (eIF2B) cause a leukoencephalopathy called vanishing white matter (VWM) disease, also known as childhood ataxia with diffuse central nervous system hypomyelination (CACH) (Schiffmann et al. 1994; Leegwater et al. 2001; van der Knaap et al. 2002). CACH/VWM disease is an autosomal recessive neurodegenerative disorder associated with > 160 mutations in eIF2B genes (OMIM#603896). The disease widely varies in onset, progression and symptoms severity, affects both genders, and has no cure. The classical form is manifested by progressive deterioration followed by death at early teens. The common denominator of all forms of the disease is progressive loss of cerebral white matter, detected by magnetic resonance imaging (MRI), leading to neurological deficits including motor dysfunction, cerebellar ataxia, and cognitive decline. An important feature is the deterioration of clinical symptoms upon exposure to environmental and physiological stressors such as febrile illness, head trauma, or acute fright. The prevalence of known living affected individuals is ~ 1.4:1,000,000 inhabitants, while the prevalence of individuals carrying two mutant alleles of a gene encoding a specific eIF2B subunit has been estimated to be 1:80,000–100,000 live births (Fogli and Boespflug-Tanguy 2006; Hamilton et al. 2018).

eIF2B is a master regulator of protein synthesis under normal and stress conditions (Pavitt 2018). It serves as a guanine nucleotide exchange factor (GEF) of eIF2, to

✉ Orna Elroy-Stein
ornaes@tauex.tau.ac.il

[1] School of Molecular Cell Biology and Biotechnology, George S. Wise Faculty of Life Sciences, Tel Aviv University, Tel Aviv, Israel

[2] Sagol School of Neuroscience, Tel Aviv University, Tel Aviv, Israel

guarantee the ongoing formation of eIF2-GTP-methionyl-tRNA ternary complex required for translation initiation. After each round of translation initiation, eIF2-GDP released from the ribosome is recycled back to eIF2-GTP by the enzymatic activity of eIF2B, to enable the next translation initiation round. Under diverse cellular stress conditions, the α subunit of eIF2 is phosphorylated by one of four protein kinases (HRI, GCN2, PKR, or PERK) depending on the stress, and turns eIF2-GDP from a substrate to a competitive inhibitor of eIF2B. The resulting lower level of ternary complexes leads to decreased global protein synthesis accompanied by effective translation of specific mRNAs encoding proteins responsible for induction of the integrated stress response (ISR). Depending on the stress severity, ISR can promote either cell rescue or apoptosis (Pavitt 2018). Hypomorphic mutations in eIF2B genes render cells hypersensitive to stress, since eIF2B enzymatic activity is already partially inhibited due to the mutation. The hyper-sensitivity of primary fibroblasts isolated from CACH/VWM patients to ER-stress (Kantor et al. 2005) and the presence of ER-stress markers in post-mortem brains (van der Voorn et al. 2005) is in agreement with this notion.

The presence of oligodendrocytes (OLG) with "foamy" cytoplasm and increased abundance of immature atypical astrocytes are major pathological hallmarks of the disease. Data collected from post-mortem brains of CACH/VWM patients demonstrated a disproportionately high number of oligodendrocyte precursor cells (OPC) compared to mature OLG, suggesting inhibition of OLG maturation as an explanation for myelin deficiency (Wong et al. 2000; Francalanci et al. 2001; Dietrich et al. 2005; Bugiani et al. 2011, 2018; Leferink et al. 2018). The observations of insufficient astrogliosis, dysmorphic immature astrocytes together with increased numbers of OPC, have led to the notion that affected astrocytes secrete unknown factor(s) causing inhibition of OLG maturation (Bugiani et al. 2018; Leferink et al. 2018). The molecular and cellular mechanisms of the disease were further analyzed following generation of mouse models (Geva et al. 2010; Dooves et al. 2016). Co-culture experiments using mixed glia isolated from Eif2b5$^{R191H/R191H}$, Eif2b4$^{R484W/R484W}$, and wild-type (WT) mice showed that eIF2B-mutant astrocytes negatively affect the development of WT OLG, while WT astrocytes support normal differentiation of mutated OLG. This phenomenon is in agreement with the notion that the OLG maturation defect, at least in part, results from malfunction of astrocytes (Dooves et al. 2016). However, it was not ruled out that mutated OPC also suffer from an inborn, cell autonomous defect due to eIF2B mutation.

The energetic requirements that OPC face during their differentiation to mature myelinating-OLG is satisfied by an increase in oxidative phosphorylation (Sanchez-Abarca et al. 2001; Rinholm et al. 2011; Schoenfeld et al. 2010). A fundamental insight related to CACH/VWM disease was the discovery of a link between eIF2B and mitochondrial function; using Eif2b5$^{R132H/R132H}$ mice we showed impaired stoichiometry between protein subunits of the electron transport chain complexes, thereby causing decreased oxidative phosphorylation (Gat-Viks et al. 2015; Raini et al. 2017). As expected, this fundamental mutation-linked outcome was observed in different cell types regardless of their involvement in the disease. However, while an increase in mitochondrial abundance corrects the phenotype of mutant fibroblasts, it is not sufficient to compensate for the high-energy demand of astrocytes, enlightening the latter as highly sensitive to eIF2B mutations (Raini et al. 2017). In the current study we assessed the mitochondrial function and abundance of primary CD140a-expressing OPC isolated from Eif2b5$^{R132H/R132H}$ and WT newborn mice. We show that Eif2b5$^{R132H/R132H}$ OPC present: (i) a decrease in oxidative phosphorylation; (ii) an increase in mitochondrial abundance; (iii) defective maturation with impaired capacity to proceed beyond stages I and II of the differentiation process; and (iv) abnormal morphology with shorter neurites length.

Materials and Methods

Mice

Wild-type (WT; C57BL strain) and Eif2b5$^{R132H/R132H}$ (Mut; mutant) mice of both sexes were bred and housed in Tel Aviv University animal facility with 14/10 h light/dark cycle in groups of four animals per cage in individually ventilated cages (Lab Products Inc., Seaford, DE, USA) supplemented with autoclaved wood chips. Animals were fed with autoclaved rodent pellet (Koffolk 19-510; Koffolk Ltd, Petach Tikva, Israel) and sterile water ad libitum. All experimental procedures were approved by the Tel Aviv University Animal Care Committee according to national guidelines (permit #04-17-022). Breeding and genotyping were performed as previously described (Geva et al. 2010). Each generation was established by back cross of homozygous Mut with WT C57BL/6 J (Harlan Labs, Jerusalem, Israel) to prevent genetic drift.

OPC Isolation and Differentiation

OPC were isolated from newborn (P0–P2) WT and Mut mice. Brains were dissociated to single-cell suspension by papain digestion using MACS Neural Tissue Dissociation kit (Miltenyi Biotec 130-092-628) and Gentle-MACS dissociator according to the manufacturer's protocol. First, astrocytes were positively selected from the cell suspension using anti-ACSA2 MicroBead Kit (Miltenyi Biotec

130-097-678). Next, OPC were isolated from the astrocytes depleted flow-through using the anti-CD140a (PDGFRα) MicroBead Kit as recommended by the supplier (Miltenyi Biotec 130-101-502). After isolation, cells were stained with mouse CD140a-PE antibody (Miltenyi Biotec 130-102-502) for 10 min at 4 °C in the dark followed by flow cytometry analysis. Cell debris and dead cells were excluded from the analysis based on the scatter signals. The yield was 23,000 OPC per brain. OPC were seeded directly for experiments in plates pre-coated with 10 ug/mL of Poly-D-Lysine (PDL) (Sigma P0899) and maintained over-night in proliferation medium consisting of BASE medium (Dulbeco Modified Eagel's Medium containing 25 mM glucose, 2 mM L-glutamine, 100 U/mL penicillin, 100 ug/mL streptomycin, 1 mM sodium pyruvate, 5 ug/mL insulin [Sigma I6634], 5 ug/mL *N*-Acetyl-L-cysteine [Sigma A8199], 1X trace elements B [Cellgro 99-175-CI], 10 ng/mL d-Biotin [Sigma B4639], 1X B27 [Invitrogen 17504-044], 0.1 mg/mL BSA [Sigma A4161], 0.1 mg/mL transferrin [Sigma T1147], 16 µg/mL putrescine [Sigma P5780], 60 ng/mL progesterone [Sigma P8783], 40 ng/mL sodium selenite [Sigma S5261]), supplemented with 10 µg/mL CNTF [Peprotech 450-02], 4.2 mg/mL Forskolin [Sigma F6886], 10 µg/mL PDGF [Peprotech 100-13A], and 1 µg/mL NT-3 [Peprotech 450-03]. Differentiation to mature OLG was induced by a change to differentiation medium consisting of BASE medium supplemented with 10 µg/mL CNTF, 4.2 mg/mL Forskolin, and 4 µg/mL thyroid hormone T3 (Sigma T6397)] as previously described (Emery and Dugas 2013).

Measurements of Mitochondria Abundance and Oxygen Consumption Rate (OCR)

OPC plated at a density of 30,000 cells per well of a 24-well plate or 12,000 cells per well of a XF96-well cell culture microplate, both pre-coated with 10 ug/mL of PDL, were incubated in proliferation medium for 24 h followed by a change to differentiation medium. 24 h later mitochondrial abundance and oxygen consumption rate (OCR) were measured. Total DNA was extracted from the 24-wells using GenElute™ Mammalian Genomic DNA Miniprep Kit (Sigma-Aldrich G1N350) followed by quantification of mitochondrial per nuclear DNA ratio using qPCR with oligonucleotide primers specific for mitochondrial 12S rRNA and nuclear 18S rRNA genes, as previously described (Raini et al. 2017). OCR for basal respiration was measured by XF96 Extracellular Flux Analyzer (Seahorse Bioscience, Billerica, MA, USA) using the Mito Stress Test Kit (Agilent Technologies, Santa Clara, CA, USA) as recommended by the supplier and as described previously (Raini et al. 2017) using the following injections: 1 µM oligomycin (Sigma O4876), 1.5 µM FCCP (Sigma C2920), 0.5 µM antimycin A (Sigma A8674), and 0.5 µM rotenone (Sigma R8875). The OCR data were normalized per biomass, obtained by Crystal Violet staining as previously described (Heiss et al. 2014) and to mtDNA content. *P* values were calculated using two-tailed *t*-test.

Transcriptome and Proteome Data Analysis

Transcriptomes of P21 brains of WT and Eif2b5$^{R132H/R132H}$ Mut mice (Marom et al. 2011) were used to compare the distribution of Log(2) fold change (Mut vs WT) mRNA expression values of 67 OLG-specific genes (Lein et al. 2007) and 40 genes encoding OLG-differentiation markers (Dugas et al. 2006), to all the rest of the transcripts in the dataset, which served as background. Proteomes of brains of WT and Mut adult mice (Gat-Viks et al. 2015) were used to compare the distribution of Log(2) fold change (Mut vs WT) expression values of 20 OLG-upregulated and 84 OLG-downregulated differentiation markers (Gobert et al. 2009), to background proteins. *P* values were calculated using Wilcoxon's test. Transcriptome and proteome datasets of cerebellums of WT and Eif2b5$^{R191H/R191H}$ mice at the age of 6–11 weeks (pre-symptomatic phase) and 27–32 weeks (post-symptomatic phase) (Wong et al. 2019) were used to compare the distribution of Log(2) fold change (Mut vs WT) mRNA expression values of 51 OL-specific genes (Lein et al. 2007) and of 67 genes encoding ETC subunits (GO:0070469) (Ashburner et al. 2000) to the background. *P* values were calculated by Wilcoxon's test.

Immunofluorescent Staining of Brain-Derived OPC Along in Vitro Differentiation

OPC were seeded at a density of 5000 cells per well of a 4-well plate on coverslips pre-coated with 10 ug/mL of PDL and maintained over-night in proliferation medium followed by change to differentiation medium (Emery and Dugas 2013) in which the cells were maintained for 3 or 5 days. At day 3 or 5, OPC were rinsed with phosphate-buffered saline (PBS) and fixed by incubation with 4% paraformaldehyde for 10 min at room temperature. For MBP and GFAP staining, a step of permeabilization was performed by 10 min incubation in ice-cold Methanol followed by washing with PBS, before blocking for 1 h at room temperature (RT) with PBS supplemented with 5% bovine serum albumin (BSA), 0.2% Triton X-100, and 1% normal goat serum. For staining of surface antigens (A2B5, O4 and GalC), the cells were directly blocked by 1 h incubation at RT with PBS supplemented with 5% BSA and 1% normal goat serum for A2B5 and GalC or only 5% BSA for O4. The coverslips were then incubated over-night at 4 °C in humidified conditions with primary antibodies, diluted in PBS supplemented with 5% BSA for A2B5, O4 and GalC staining or with 5% BSA and 0.2% Triton X-100 for MBP and GFAP staining. Incubation with O4 antibodies was performed

for 1 h at RT. The cells were then washed with PBS followed by incubation with the appropriate fluorescently-labeled secondary antibodies in PBS supplemented with either 5% BSA (for A2B5, O4 or GalC staining) or with 5% BSA and 0.2% Triton X-100 (for MBP and GFAP staining) for 1 h at RT in the dark. Following three washes with PBS, the coverslips were mounted onto glass slides using Prolong Gold Antifade Reagent with DAPI (Molecular Probes P36935). The following primary and secondary antibodies were used: mouse anti-A2B5 (R&D Systems MAB1416, 1:50); mouse anti-O4 (R&D Systems MAB1326, 1:25); rabbit anti-GalC (Sigma G9152, 1:500); chicken anti-MBP (Millipore AB9348, 1:100), rabbit anti-GFAP (Dako Z0334, 1:2000), AlexaFluor-488 donkey anti-mouse IgG (Abcam ab150109, 1:1000), AlexaFluor-555 goat anti-rabbit IgG (Abcam ab150086, 1:1000), AlexaFluor-555 goat anti-chicken IgY (Abcam ab150170, 1:1000), and AlexaFluor-488 goat anti-rabbit (Invitrogen A11034, 1:1000). 10X Images were captured using Nikon Eclipse 50i microscope. Identical exposure time was used for each marker in each independent experiment. Each differentiation stage was evaluated by assessment of morphology and markers expression. Quantification of cells in each stage was performed by manual counting the number of positive cells for each specific marker, normalized to the total number of cells assessed by DAPI. ~ 80 cells per field were counted, using 10 different fields in each experiment. *P* values were calculated using two-tailed t-test.

Live-Cell Imaging and Analysis of Differentiating OPC

OPC were seeded at a density of 5,000 cells per well of a 96-well Corning plate pre-coated with 10 ug/mL of PDL and maintained over-night in proliferation medium followed by change to differentiation medium and further incubated in IncuCyte ZOOM incubator. Morphological changes along the differentiation process were monitored by automatic capture of 10X images at 45 min intervals. The images were then analyzed using IncuCyte NeuroTrack software to assess neurite length (NL) and neurite branch points (NBP). NBP were normalized per cell number quantified by ImageJ software. *P* values were calculated using two-tailed t-test.

Results

Primary OPC Isolated from Eif2b5$^{R132H/R132H}$ Mice Exhibit Defective Mitochondrial Function

The challenging energy metabolism of astrocytes involves excessive rates of oxidative respiration and glycolysis (Belanger et al. 2011). Likewise, OLG depend on mitochondrial functions and increased energy demands during differentiation and myelination (Sanchez-Abarca et al. 2001; Rinholm et al. 2011; Schoenfeld et al. 2010). In previous studies, we used Eif2b5$^{R132H/R132H}$ (Mut) mice to demonstrate the negative effect of mutated eIF2B on oxidative respiration and mitochondrial performance in whole brain tissue, cultured primary astrocytes, and cultured primary mouse embryonic fibroblasts (MEFs) (Gat-Viks et al. 2015; Raini et al. 2017). To test if Mut OPC have the necessary energy produced by mitochondrial oxidative phosphorylation during their differentiation, CD140a-positive OPC were isolated from WT and Eif2b5$^{R132H/R132H}$ (Mut) mice. The low abundance (3–8% in the brain of newborn rodents) and high sensitivity of OLG turn their isolation and maintenance into a challenging task in terms of yield and viability. Using immuno-selection, we first depleted the astrocytes by negative selection, followed by pulling CD140a-expressing OPC from the flow-through by positive selection. Our cultures contained > 80% CD140a-positive cells, < 2% astrocytes, and some other cell types including fibroblasts (Fig. 1a, left panel). The cells were incubated in OPC proliferation medium, followed by addition of thyroid hormone 24 h later to induce differentiation. Following 24 h in differentiation medium, mitochondrial DNA content and oxygen consumption rate (OCR) were quantified. The data show 1.36-fold increase in mitochondria abundance in Mut compared to WT cultures (Fig. 1b, left panel). The increase in mitochondria abundance is attributed primarily to OPC, since the presence of other cell types (<20%) in the cultures cannot account for such an increase, based on our previous study related to MEFs and astrocytes (Raini et al. 2017). In addition to the increase in mitochondrial biogenesis in Mut OPC, the data show a 30% decrease in basal oxidative respiration rate per cell in Mut compared to WT OPC, despite the increase in mitochondria abundance (Fig. 1b, middle panel). The 50% decrease in basal oxidative respiration per mitochondria in Mut OPC (Fig. 1b, right panel) clearly reflects their defective oxidative phosphorylation due to the mutation in eIF2B. This observation evidently demonstrates the mal-adaptation of Mut OPC to differentiation-linked high-energy requirements, as reflected by increased mitochondria abundance and yet only partial compensation for mitochondrial dysfunction. The inability of Mut OPC to produce sufficient available energy has raised the query about the efficiency of their differentiation into mature OLG, since it is a high-energy demanding process (Sanchez-Abarca et al. 2001; Rinholm et al. 2011; Schoenfeld et al. 2010).

Primary Eif2b5$^{R132H/R132H}$ OPC Present Impaired Differentiation Capacity and Abnormal Morphology

In a previous study, we focused on the transcriptomes of brains isolated from WT and Mut mice at the peak

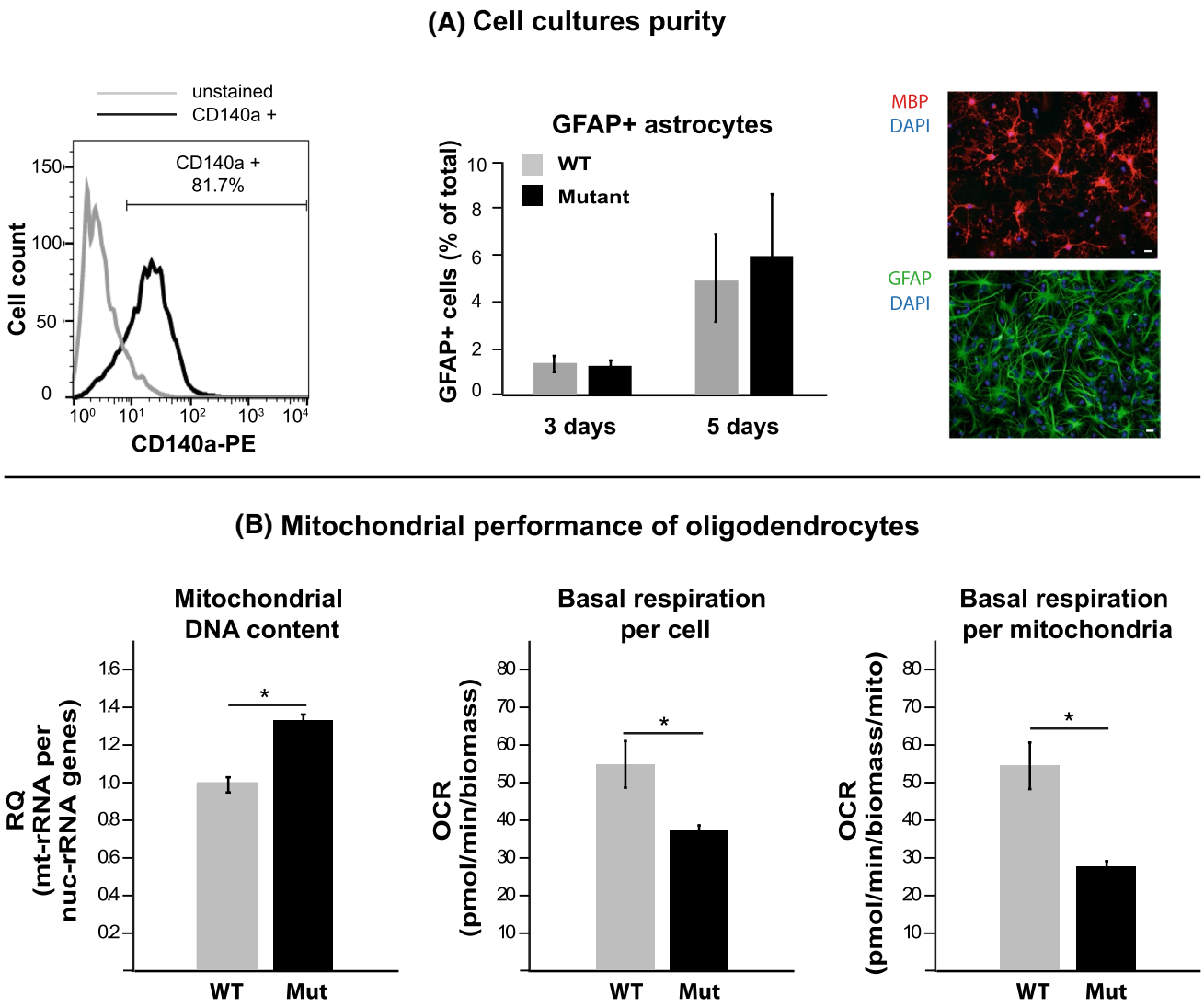

Fig. 1 Primary OPC isolated from Eif2b5$^{R132H/R132H}$ mice exhibit impaired mitochondrial function. **a** Left panel: a representative flow cytometry analysis of OPC sample following isolation from newborn mice brains. Black, CD140a-expressing cells (81.7% of the cells are CD140a-positive); gray, unstained control. Middle panel: OPC isolated from WT (gray) and Mut (black) mice and incubated for 3 and 5 days in differentiation medium were stained for GFAP. Shown is the average ± SEM of 4 independent experiments. Note the presence of < 2% and < 6% astrocytes after 3 and 5 days, respectively. Right panel: a representative image of CD140a-selected OPC grown for 3 days in OPC differentiation medium followed by staining for MBP (red, top; note that most of the cells in the culture are OLG), and ACSA2-selected astrocytes followed by staining for GFAP marker (green, bottom; note the different morphology of astrocytes). DAPI (blue) used for nuclear staining. Scale bar, 10 µm. **b** Left panel: qPCR analysis of mitochondrial and nuclear DNA encoding mitochondrial 12S rRNA and nuclear 18S rRNA genes, respectively. Shown is average relative quantity (RQ) of three independent experiments normalized to WT ± SEM. *$P < 0.05$, two-tailed t-test. Middle and right panels show oxygen consumption rate (OCR) at 24 h of differentiation. Shown is pmol of oxygen consumed per minute for basal respiration, normalized to biomass (middle) or to biomass and mtDNA content (right). Bars represent average values ± SEM of 6 replicates in a representative experiment. *$P < 0.05$, two-tailed t-test

of myelin formation (P21). We reported > 400 differentially expressed mRNAs in Mut compared to WT brains (Marom et al. 2011). Further comparison of this dataset (21,909 transcripts) to genome-wide expression atlas of adult mouse brain (Lein et al. 2007) and to another dataset of OLG differentiation (Dugas et al. 2006), revealed significant down regulation of 67 OLG-specific mRNAs and 40 OLG-differentiation mRNAs in Mut compared to WT brains (Fig. 2a, left panel), supporting impaired differentiation of OPC due to eIF2B mutation. To further corroborate this insight, we checked the differential gene expression at the protein level. For this purpose, we used our proteomic dataset generated from adult WT and Mut brains (Gat-Viks et al. 2015) to check Mut/WT fold

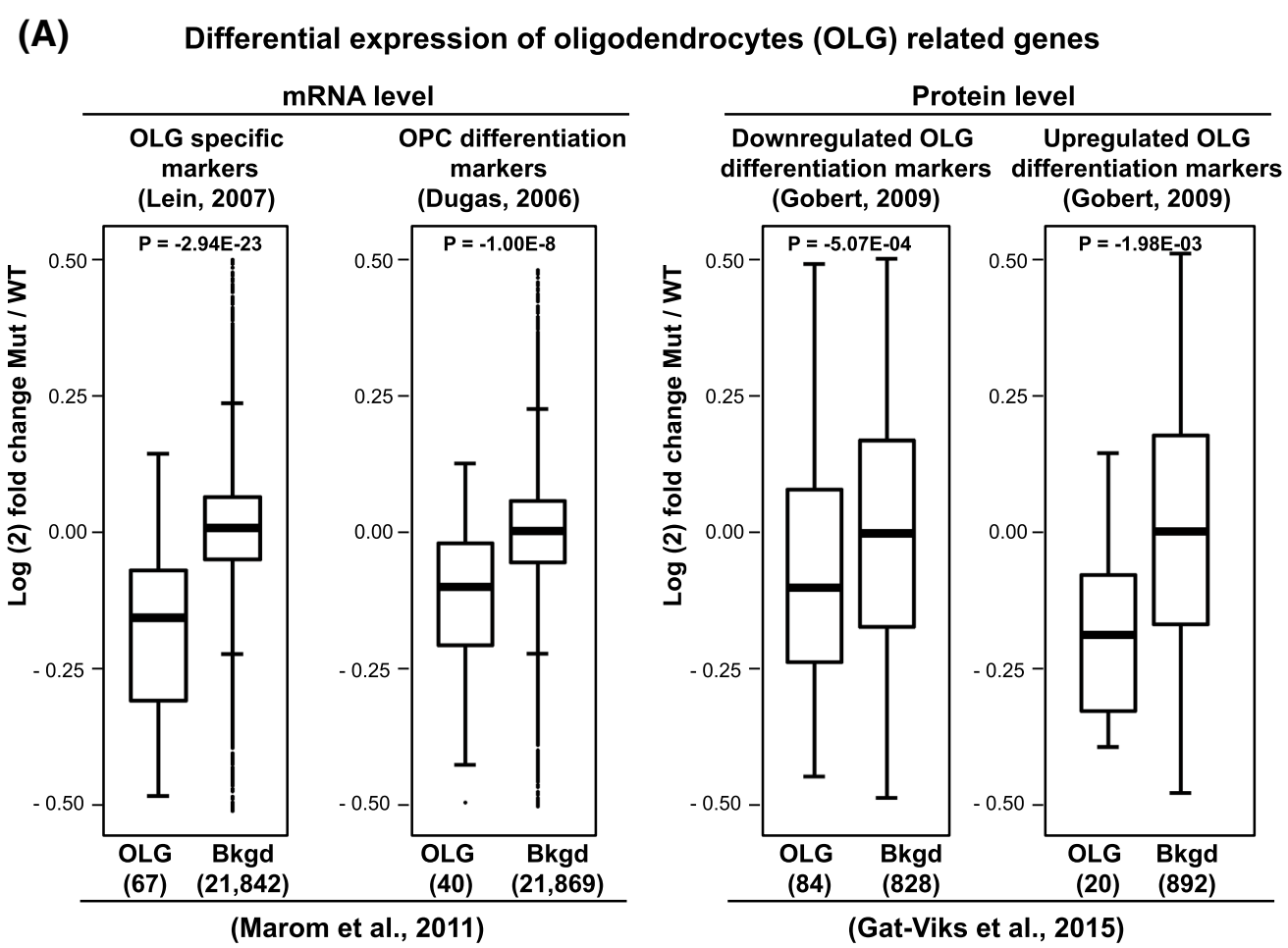
(A)
Differential expression of oligodendrocytes (OLG) related genes
mRNA level
Protein level
OLG specific markers (Lein, 2007)
OPC differentiation markers (Dugas, 2006)
Downregulated OLG differentiation markers (Gobert, 2009)
Upregulated OLG differentiation markers (Gobert, 2009)
P = -2.94E-23
P = -1.00E-8
P = -5.07E-04
P = -1.98E-03
Log (2) fold change Mut / WT
0.50
0.25
0.00
- 0.25
- 0.50
OLG (67)
Bkgd (21,842)
OLG (40)
Bkgd (21,869)
OLG (84)
Bkgd (828)
OLG (20)
Bkgd (892)
(Marom et al., 2011)
(Gat-Viks et al., 2015)

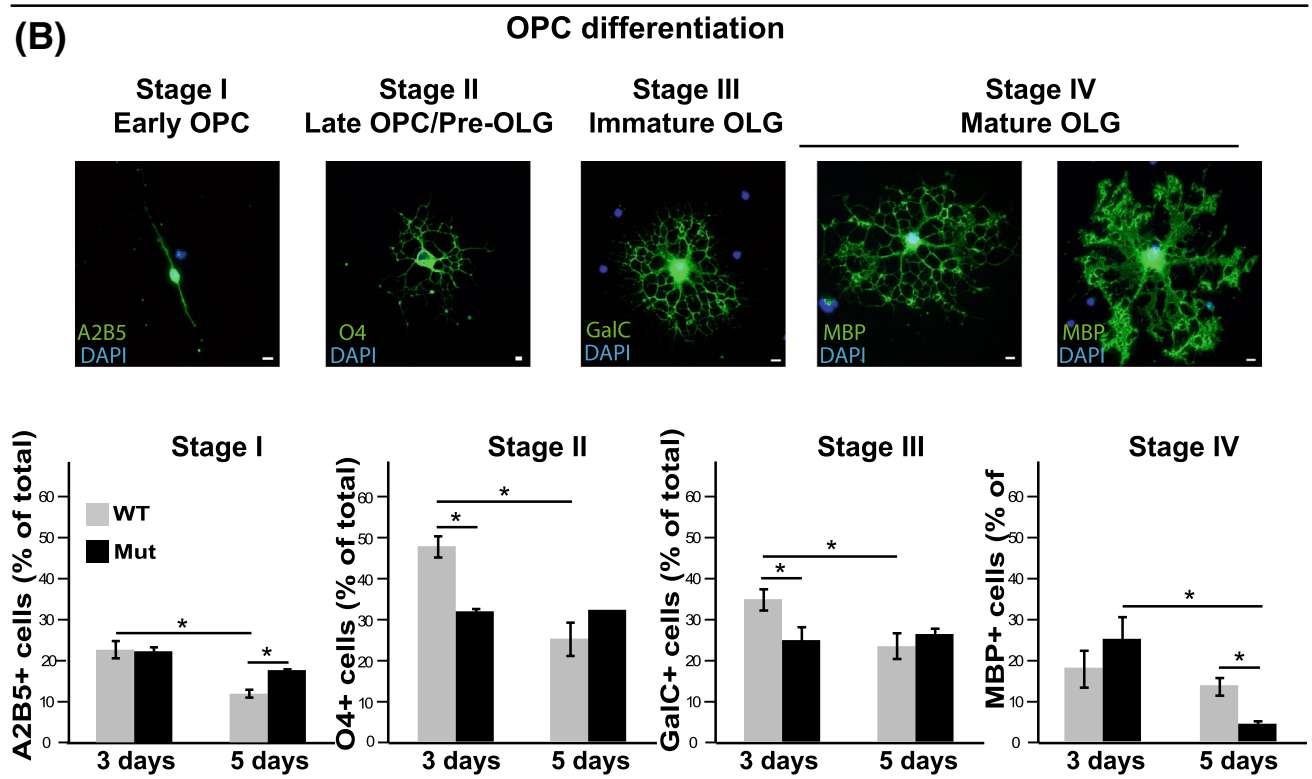
(B)
OPC differentiation
Stage I Early OPC
Stage II Late OPC/Pre-OLG
Stage III Immature OLG
Stage IV Mature OLG
A2B5 DAPI
O4 DAPI
GalC DAPI
MBP DAPI
MBP DAPI
Stage I
Stage II
Stage III
Stage IV
WT
Mut
A2B5+ cells (% of total)
O4+ cells (% of total)
GalC+ cells (% of total)
MBP+ cells (% of
0
10
20
30
40
50
60
*
3 days
5 days

◂**Fig. 2** Differentiation of Eif2b5$^{R132H/R132H}$ OLG is impaired. **a** Datasets analyses. Left panel: Analysis of the transcriptome dataset of P21 brains of WT and Mut mice (Marom et al. 2011). Shown is the distribution of Log(2) fold change (Mut vs WT) mRNA expression values of 67 OLG-specific genes (Lein et al. 2007) (left) and of 40 genes encoding OLG-differentiation markers (Dugas et al. 2006) (right), compared to background. Right panel: Analysis of proteome dataset of brains harvested from adult WT and Mut mice (Gat-Viks et al. 2015). Shown is the distribution of Log(2) fold change (Mut vs WT) expression values of 20 OLG-upregulated differentiation markers (right) and 84 OLG-downregulated differentiation markers (left) (Gobert et al., 2009), compared to background. *P* values calculated by Wilcoxon's test. **b** OPC isolated from WT (gray) and Mut (black) newborn mice cultured in differentiation media for 3 or 5 days followed by immunofluorescent staining with antibodies specific for A2B5, O4, GalC and MBP, as indicated. DAPI (blue) was used for nuclear staining. Shown are representative images (×40) of WT OPC along I–IV differentiation stages (top). Scale bar, 10 µm. % of positive cells for each differentiation marker at day 3 and day 5 was quantified within total of > 300 WT (gray) and Mut (black) cells. Shown is the average ± SEM of 4 independent experiments. $*P < 0.05$, two-tailed t-test (bottom)

change of 20 and 84 markers that had been reported to be up- or down- regulated, respectively, during OLG differentiation (Gobert et al. 2009). The comparison revealed significant down regulation of both groups of proteins in Mut compared to WT brains (Fig. 2a, right panel), which could imply either lower expression per cell of such differentiation-related proteins or overall lower number of mature OLG in adult brains due to eIF2B mutation. To confirm the predicted faulty differentiation process of OLG and test if this feature is an autonomous defect of eIF2B-mutated OPC regardless of astrocytes involvement, we induced in vitro differentiation of OPC isolated from WT and Mut newborn mice brains to mature OLG (Emery and Dugas 2013). OPC differentiation to myelinating-OLG is a complex process involving changes in morphology, specific gene expression programs (Buchet and Baron-Van Evercooren 2009) and epigenetic modifications (Liu et al. 2010). After 3 and 5 days in specialized differentiation medium, the differentiation status of the cells was assessed by morphology and expression of A2B5, O4, GalC, and MBP markers, which are typically expressed along four rudimentary differentiation stages (Buchet and Baron-Van Evercooren 2009). According to this crude classification, bipolar morphology and A2B5 expression represent early OPC (stage I); Multipolar morphology with short processes and O4 expression represent late OPC/pre-OLG (stage II); Multipolar morphology with long and ramified branches and Gal C expression represent immature OLG (stage III); and myelin sheaths morphology with MBP expression represent mature OLG (stage IV) (Fig. 2b, upper panel). Since expression gain/loss of these representative markers is gradual, cells between consecutive stages simultaneously express two markers, explaining a sum of > 100% in cell counts according to the above-chosen stage specification. Importantly, the presence of GFAP-positive cells in the differentiating OPC cultures did not exceed 8% at all times (Fig. 1a, middle panel). Even though a large number of both WT and Mut OPC could not survive the 5 days experiment, it was clear that WT OPC are able to exhibit the expected drop in A2B5, O4, and Gal C expression as they proceed from day 3 to day 5, while similar changes were not observed in Mut OPC (Fig. 2b, bottom panel), suggesting a slower differentiation process of Mut OPC. The lower percentage of O4-positive stage II Mut OPC compared to WT at day 3, and the higher percentage of A2B5-positive stage I Mut OPC compared to WT at day 5, is consistent with their lagging progression from stage I to stage II. Similarly, the lack of decreased percentage of O4-positive stage II Mut OPC compared to WT from day 3 to day 5, is consistent with their lagging progression from stage II to stage III. The marked decrease in Mut MBP-positive stage IV-mature OLG from day 3 to day 5 implicates their higher sensitivity and vulnerability compared to WT (Fig. 2b, bottom panel). To analyze the morphological aspects of Mut OLG along their differentiation process, OPC cultures maintained in differentiation medium were continuously visualized along 3-days. A representative image of a typical Mut OPC culture in differentiation medium is shown in Fig. 1a (right panel, top). Note the different morphology of astrocytes, which is not observed in the OPC cultures (Fig. 1a, right panel, bottom). Automatic image capturing followed by computerized analyses of neurite branch points (NBP) and neurite length (NL) revealed an increase in both parameters until 62 h, a time point at which both parameters started to decrease as an indication of viability decay of the cultures. Within the first 62 h in culture, both WT and Mut OPC produced the same number of NBP per cell (Fig. 3, left panel) however Mut OPC had shorter NL at each time point (Fig. 3, right panel). Moreover, while the WT steady increase in NL reached plateau around 40 h, Mut OPC did not exhibit a plateau of this parameter during the entire duration of the experiment. This observation is in agreement with an abnormal morphology in OLG due to the mutation in eIF2B.

Impaired Oxidative Respiration is Verified by Omics Analysis of an Additional VWM Mouse Model Harboring a Different Mutation in eIF2B

Transcriptome and proteome datasets of cerebellums of WT and Eif2B5$^{R191H/R191H}$ mice (Dooves et al. 2016) were recently published (Wong et al. 2019). Analysis of these datasets provided an additional support to our findings related to the effect of mutated eIF2B on the mitochondrial respiratory chain complex. The analysis revealed a significant lower abundance of ETC-related gene products on the

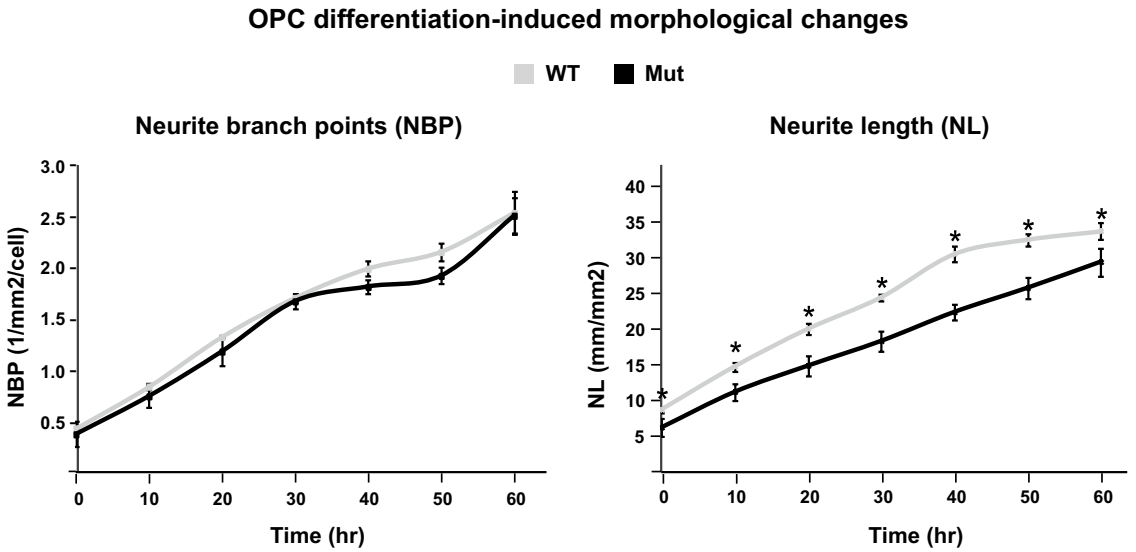

Fig. 3 Abnormal morphology in Eif2b5$^{R132H/R132H}$ OPC. OPC isolated from WT (gray) and Mut (black) mice. Morphological changes monitored by continuous imaging along 62 h in IncuCyte ZOOM incubator, starting at differentiation medium addition. Shown is average of Neurite length and Neurite branch points/cell per time point ± SEM. 5000 cells were analyzed per each of 4 replicates. *$P < 0.05$, two-tailed t-test

mRNA level at both pre-symptomatic (6-11 weeks) and post-symptomatic (27–32 weeks) phases. The proteomics data, obtained only from 27–32 weeks old mice, also show a similar trend (Fig. 4, upper panel). These data further support oxidative phosphorylation dysfunction in VWM disease, as was claimed earlier for Eif2B5$^{R132H/R132H}$ mice (Raini et al. 2017; Elroy-Stein 2017). Importantly, further analysis of Eif2B5$^{R191H/R191H}$ datasets also revealed down regulation, in both pre- and post- symptomatic phases, of OLG-specific markers (Lein et al. 2007) (Fig. 4, lower panel), as reflected in the Eif2b5$^{R132H/R132H}$ transcriptome (Fig. 2a, left panel).

Discussion

Mitochondrial Dysfunction in VWM Disease

Previously we provided evidence that a mild mutation in the catalytic subunit of eIF2B leading to ~ 20% decrease in its enzymatic activity (Geva et al. 2010) is associated with defective mitochondrial oxidative respiration in primary MEFs and astrocytes. We also showed that both cell types employ a compensatory response of increased mitochondria abundance in order to meet energy requirements. However, while this adaptive approach is sufficient for Mut MEFs, it is not the case for Mut astrocytes which exhibit three-fold lower oxidative respiration per cell despite ~ two-fold higher mtDNA content compared to WT, explaining the involvement of astrocytes but not fibroblasts in the disease (Elroy-Stein 2017; Raini et al. 2017). These findings are in agreement with abnormal expression level of proteins involved in oxidative phosphorylation, found by unbiased proteomic analyses using whole brains and primary MEFs isolated from the Eif2B5$^{R132H/R132H}$ mice (Gat-Viks et al. 2015; Raini et al. 2017). The low expression level of respiratory proteins in brains isolated from Eif2B5$^{R191H/R191H}$ mice harboring a more severe eIF2B mutation (Wong et al. 2019 and Fig. 4), together with their more severe clinical signs (Wong et al., 2019), further support our insight related to the association of eIF2B mutations with mitochondria malfunction. The current study provides evidence that eIF2B-mutant OPC suffer from mitochondrial malfunction (Fig. 1). As in the case of Mut primary astrocytes, the increase in mitochondria abundance observed in Mut OPC is probably not sufficient to fully compensate for their defective basal oxidative respiration, known to be important for efficient differentiation to mature OLG. The abnormal morphology exhibited by shorter neurites length and the lack of ability to gain sufficient O4 expression required for passing a critical differentiation step provide evidence for the mal differentiation of Mut OPC (Figs. 2, 3). The notion that the defective differentiation could be a consequence of mitochondrial malfunction is in agreement with numerous studies indicating high dependency of differentiating OLG on accurate mitochondrial performance and ATP availability. The transition from OPC to mature myelinating-OLG relies on extensive mitochondrial respiration. This renders differentiating OLG especially dependent on mitochondrial biogenesis and particularly sensitive to mitochondrial inhibition (Sanchez-Abarca et al., 2001, Schoenfeld et al., 2010, Rinholm et al.,

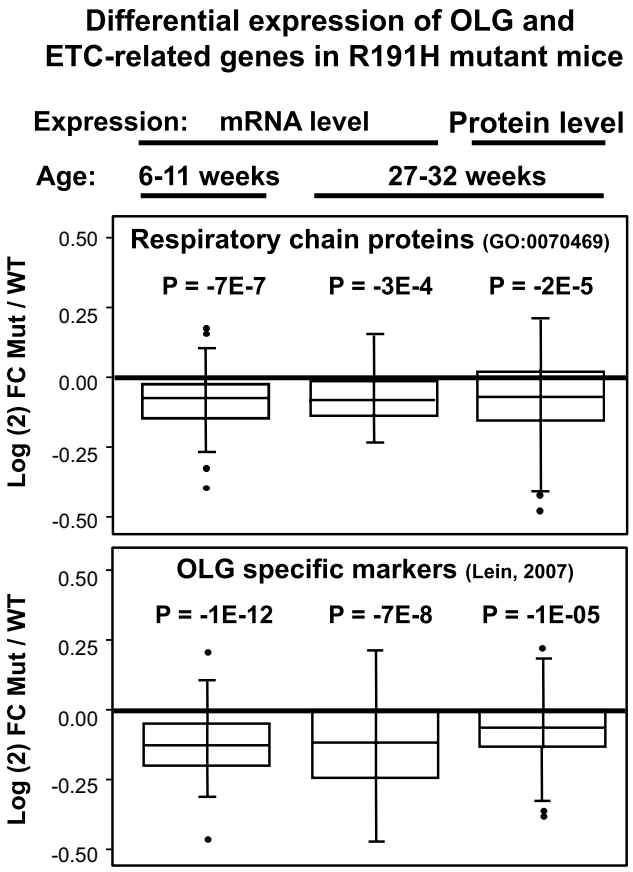

Fig. 4 Defective OLG differentiation and mitochondrial function in Eif2b5$^{R191H/R191H}$ mice. Analysis of transcriptome and proteome datasets of mRNAs and proteins isolated from the cerebellum of Eif2b5$^{R191H/R191H}$ (Mut) and WT mice at pre-symptomatic (6–11 weeks) and post-symptomatic (27–32 weeks) phases (Wong et al. 2019). Shown is the distribution of Log(2) fold change (Mut vs WT) values of the products of 67 genes encoding respiratory chain proteins (GO:0070469) (Ashburner et al. 2000) (top), and 51 OLG-specific genes (Lein et al. 2007) compared to the background. *P* values were calculated by Wilcoxon's test

2011). The ATP requirement for myelin sheath formation in vivo (Bizzozero et al. 1999) and the impaired differentiation of neural stem cells to OLG upon genetic mitochondrial impairment (Diaz-Castro et al. 2015) further support this concept. The connection between mitochondrial membrane potential interference in mature OLG by the copper chelator cuprizone, further underlines the importance of proper mitochondrial function for remyelination (Benardais et al. 2013). The defective differentiation of Mut OPC observed in the current study is in line with the involvement of OLG in CACH/VWM disease, as reflected by the disproportionately high number of OPC compared to mature OLG in patients, explanation for the continuous loss of white matter and myelin deficiency (Van Haren et al. 2004; van der Knaap et al. 2006; Rodriguez et al. 1999; Wong et al. 2000; Bugiani et al. 2011; Leferink et al. 2018).

Mitochondrial dysfunction is generally regarded as a secondary phenomenon caused by cellular dysfunction in multiple neurodegenerative diseases. However, we believe that this is not the case for VWM disease, which is caused by mutations in eIF2B, a master regulator of cytoplasmic protein synthesis. While only 37 genes (encoding rRNA, tRNA and 13 proteins) constitute the mitochondrial genome, > 1000 nuclear genes encode the rest of the mitochondrial proteins, which include hundreds that play important roles in oxidative respiration and the mitochondrial translation machinery itself (Taanman 1999; Vafai and Mootha 2012; Calvo et al. 2015). The expression from both genomes must be tightly coordinated to adapt mitochondrial content and performance to cellular energetic requirements (Jacobs and Turnbull 2005; Quiros et al. 2016). It seems that eIF2B functions as an important coordinator (Elroy-Stein 2017). Hypomorphic mutations in eIF2B leading to partial loss of its enzymatic activity are associated with hyper-active ISR, increased ER-stress (induced by hyperactivity of PERK arm in the absence of appropriate coordination with the IRE-1 and ATF6 arms), and eventually increased mitochondrial stress (Kerkhofs et al. 2018). We believe this cellular scenario occurs in all types of cells upon eIF2B mutations. However, some cell types are more sensitive than others with glial cells being the most sensitive of all. Strong support to this concept is provided by the following findings: (i) fibroblasts, representing cell types that are not involved in the disease, also suffer from impaired mitochondrial function; and (ii) there is a low expression level of proteins involved in oxidative respiration in brains of Eif2B5$^{R191H/R191H}$ mice at a pre-symptomatic age.

The Mechanistic Role of Astrocytes in CACH/VWM Disease Remains an Open Question

The current study widens the angle of the existing view about the role of astrocytes in CACH/VWM disease. While astrocytes were marked as central for the disease, it was suggested that eIF2B-mutant OLG lack a cellular phenotype on their own (Dooves et al. 2016). The correlation between the enrichment of CD44-expressing astrocytes and accumulation of high molecular weight (HMW) hyaluronan, especially in the demyelinated brain areas, has led to the suggestion that HMW hyaluronan is responsible for the glial maturation inhibition and white matter pathology (Bugiani et al. 2013). However, since high hyaluronan levels correlate only with the late, more severe stages of the pathology observed in Eif2b5$^{R191H/R191H}$ mouse model, it could not explain the inhibitory effect on OLG maturation at earlier stages of the disease.

Importantly, the study of Lin et al. (2014) provides an additional indication in favor of an intrinsic defect in OLG due to eIF2B mutation. This study clearly links PERK activation specifically in OLG during early development, with activation of ISR and induction of symptoms highly reminiscent of CACH/VWM (Lin et al. 2014). This observation suggests an autonomous role of OLG in the disease, particularly in conjunction with cellular stress related to hyper-activation of the ISR arm of UPR, as expected from eIF2B hypomorphic mutations. In line with this notion is the significant enrichment of ISR markers specifically in myelinating-OLG, as obtained by single-cell mRNA sequencing of cells isolated from $Eif2b5^{R191H/R192H}$ mice brains (Wong et al. 2019), given the well-known reciprocal link between ER-stress and mitochondrial stress (Kerkhofs et al. 2018). Although the defective differentiation of Mut OPC observed in the current study cannot be explained by the presence of < 8% astrocytes in our OPC cultures, the possibility that astrocytes are solely responsible for this effect cannot be completely ruled out. Since previous co-culture experiments suggested the ability of factors secreted from WT astrocytes to mediate normal maturation of mutant OLG (Dooves et al. 2016), future experiments will hopefully assess the ability of such factors to overcome the energetic deficits generated in OPC due to mutation in eIF2B.

Acknowledgements This study was funded by the U.S.-Israel Binational Science Foundation (BSF) Grant #2009159 and by the VWM Saxby project grant to OES.

Compliance with Ethical Standards

Conflict of interest The authors declare that the research was conducted in the absence of any commercial or financial relationships that could be construed as a potential conflict of interest.

Ethical Approval All procedures performed in studies involving animals were in accordance with the ethical standards of Tel Aviv University Animal Care Committee according to national guidelines (permit #04-17-022). This article does not contain any studies with human participants performed by any of the authors.

References

Ashburner, M., Ball, C. A., Blake, J. A., Botstein, D., Butler, H., Cherry, J. M., et al. (2000). Gene ontology: Tool for the unification of biology. *Nature Genetics, 25*(1), 25.

Belanger, M., Allaman, I., & Magistretti, P. J. (2011). Brain energy metabolism: Focus on astrocyte-neuron metabolic cooperation. *Cell Metabolism, 14*(6), 724–738.

Benardais, K., Kotsiari, A., Skuljec, J., Koutsoudaki, P. N., Gudi, V., Singh, V., et al. (2013). Cuprizone [bis(cyclohexylidenehydrazide)] is selectively toxic for mature oligodendrocytes. *Neurotoxicity Research, 24*(2), 244–250.

Bizzozero, O. A., Sanchez, P., & Tetzloff, S. U. (1999). Effect of ATP depletion on the palmitoylation of myelin proteolipid protein in young and adult rats. *Journal of Neurochemistry, 72*(6), 2610–2616.

Buchet, D., & Baron-Van Evercooren, A. (2009). In search of human oligodendroglia for myelin repair. *Neuroscience Letters, 456*(3), 112–119.

Bugiani, M., Boor, I., van Kollenburg, B., Postma, N., Polder, E., van Berkel, C., et al. (2011). Defective glial maturation in vanishing white matter disease. *Journal of Neuropathology and Experimental Neurology, 70*(1), 69–82.

Bugiani, M., Postma, N., Polder, E., Dieleman, N., Scheffer, P. G., Sim, F. J., et al. (2013). Hyaluronan accumulation and arrested oligodendrocyte progenitor maturation in vanishing white matter disease. *Brain, 136*(Pt 1), 209–222.

Bugiani, M., Vuong, C., Breur, M., & van der Knaap, M. S. (2018). Vanishing white matter: A leukodystrophy due to astrocytic dysfunction. *Brain Pathology, 28*(3), 408–421.

Calvo, S. E., Clauser, K. R., & Mootha, V. K. (2015). MitoCarta2.0: An updated inventory of mammalian mitochondrial proteins. *Nucleic Acids Research, 44,* 1251–1257. https://doi.org/10.1093/nar/gkv1003.

Diaz-Castro, B., Pardal, R., Garcia-Flores, P., Sobrino, V., Duran, R., Piruat, J. I., et al. (2015). Resistance of glia-like central and peripheral neural stem cells to genetically induced mitochondrial dysfunction-differential effects on neurogenesis. *EMBO Reports*. 10.15252/embr.201540982.

Dietrich, J., Lacagnina, M., Gass, D., Richfield, E., Mayer-Proschel, M., Noble, M., et al. (2005). EIF2B5 mutations compromise GFAP+ astrocyte generation in vanishing white matter leukodystrophy. *Nature Medicine, 11*(3), 277–283.

Dooves, S., Bugiani, M., Postma, N. L., Polder, E., Land, N., Horan, S. T., et al. (2016). Astrocytes are central in the pathomechanisms of vanishing white matter. *The Journal of clinical investigation, 126*(4), 1512–1524.

Dugas, J. C., Tai, Y. C., Speed, T. P., Ngai, J., & Barres, B. A. (2006). Functional genomic analysis of oligodendrocyte differentiation. *Journal of Neuroscience, 26*(43), 10967–10983.

Elroy-Stein, O. (2017). Mitochondrial malfunction in vanishing white matter disease: A disease of the cytosolic translation machinery. *Neural Regeneration Research, 12*(10), 1610–1612.

Emery, B., & Dugas, J. C. (2013). Purification of oligodendrocyte lineage cells from mouse cortices by immunopanning. *Cold Spring Harbor Protocols, 2013*(9), 854–868.

Fogli, A., & Boespflug-Tanguy, O. (2006). The large spectrum of eIF2B-related diseases. *Biochemical Society Transactions, 34*(Pt 1), 22–29.

Francalanci, P., Eymard-Pierre, E., Dionisi-Vici, C., Boldrini, R., Piemonte, F., Virgili, R., et al. (2001). Fatal infantile leukodystrophy: A severe variant of CACH/VWM syndrome, allelic to chromosome 3q27. *Neurology, 57*(2), 265–270.

Gat-Viks, I., Geiger, T., Barbi, M., Raini, G., & Elroy-Stein, O. (2015). Proteomics-level analysis of myelin formation and regeneration in a mouse model for vanishing white matter disease. *Journal of Neurochemistry, 134*(3), 513–526.

Geva, M., Cabilly, Y., Assaf, Y., Mindroul, N., Marom, L., Raini, G., et al. (2010). A mouse model for eukaryotic translation initiation factor 2B-leucodystrophy reveals abnormal development of brain white matter. *Brain, 133*(Pt 8), 2448–2461.

Gobert, R. P., Joubert, L., Curchod, M. L., Salvat, C., Foucault, I., Jorand-Lebrun, C., et al. (2009). Convergent functional genomics of oligodendrocyte differentiation identifies multiple autoinhibitory signaling circuits. *Molecular and Cellular Biology, 29*(6), 1538–1553.

Hamilton, E. M. C., van der Lei, H. D. W., Vermeulen, G., Gerver, J. A. M., Lourenco, C. M., Naidu, S., et al. (2018). Natural history of vanishing white matter. *Annals of Neurology, 84*(2), 274–288.

Heiss, E. H., Kramer, M. P., Atanasov, A. G., Beres, H., Schachner, D., & Dirsch, V. M. (2014). Glycolytic switch in response to betulinic acid in non-cancer cells. *PLoS ONE, 9*(12), e115683.

Jacobs, H. T., & Turnbull, D. M. (2005). Nuclear genes and mitochondrial translation: A new class of genetic disease. *Trends in Genetics, 21*(6), 312–314.

Kantor, L., Harding, H. P., Ron, D., Schiffmann, R., Kaneski, C. R., Kimball, S. R., et al. (2005). Heightened stress response in primary fibroblasts expressing mutant eIF2B genes from CACH/VWM leukodystrophy patients. *Human Genetics, 118*(1), 99–106.

Kerkhofs, M., Bittremieux, M., Morciano, G., Giorgi, C., Pinton, P., Parys, J. B., et al. (2018). Emerging molecular mechanisms in chemotherapy: Ca(2+) signaling at the mitochondria-associated endoplasmic reticulum membranes. *Cell Death & Disease, 9*(3), 334.

Leegwater, P. A., Vermeulen, G., Konst, A. A., Naidu, S., Mulders, J., Visser, A., et al. (2001). Subunits of the translation initiation factor eIF2B are mutant in leukoencephalopathy with vanishing white matter. *Nature Genetics, 29*(4), 383–388.

Leferink, P. S., Breeuwsma, N., Bugiani, M., van der Knaap, M. S., & Heine, V. M. (2018). Affected astrocytes in the spinal cord of the leukodystrophy vanishing white matter. *Glia, 66*(4), 862–873.

Lein, E. S., Hawrylycz, M. J., Ao, N., Ayres, M., Bensinger, A., Bernard, A., et al. (2007). Genome-wide atlas of gene expression in the adult mouse brain. *Nature, 445*(7124), 168–176.

Lin, Y., Pang, X., Huang, G., Jamison, S., Fang, J., Harding, H. P., et al. (2014). Impaired eukaryotic translation initiation factor 2B activity specifically in oligodendrocytes reproduces the pathology of vanishing white matter disease in mice. *Journal of Neuroscience, 34*(36), 12182–12191.

Liu, J., & Casaccia, P. (2010). Epigenetic regulation of oligodendrocyte identity. *Trends in Neurosciences, 33*(4), 193–201.

Marom, L., Ulitsky, I., Cabilly, Y., Shamir, R., & Elroy-Stein, O. (2011). A point mutation in translation initiation factor eIF2B leads to function–and time-specific changes in brain gene expression. *PLoS ONE, 6*(10), e26992.

Pavitt, G. D. (2018). Regulation of translation initiation factor eIF2B at the hub of the integrated stress response. *Wiley Interdisciplinary Reviews: RNA, 9*(6), e1491.

Quiros, P. M., Mottis, A., & Auwerx, J. (2016). Mitonuclear communication in homeostasis and stress. *Nature Reviews Molecular Cell Biology, 17*(4), 213–226.

Raini, G., Sharet, R., Herrero, M., Atzmon, A., Shenoy, A., Geiger, T., et al. (2017). Mutant eIF2B leads to impaired mitochondrial oxidative phosphorylation in vanishing white matter disease. *Journal of Neurochemistry, 141*(5), 694–707.

Rinholm, J. E., Hamilton, N. B., Kessaris, N., Richardson, W. D., Bergersen, L. H., & Attwell, D. (2011). Regulation of oligodendrocyte development and myelination by glucose and lactate. *Journal of Neuroscience, 31*(2), 538–548.

Rodriguez, D., Gelot, A., Della Gaspera, B., Robain, O., Ponsot, G., Sarlieve, L. L., et al. (1999). Increased density of oligodendrocytes in childhood ataxia with diffuse central hypomyelination (CACH) syndrome: Neuropathological and biochemical study of two cases. *Acta Neuropathologica, 97*(5), 469–480.

Sanchez-Abarca, L. I., Tabernero, A., & Medina, J. M. (2001). Oligodendrocytes use lactate as a source of energy and as a precursor of lipids. *Glia, 36*(3), 321–329.

Schiffmann, R., Moller, J. R., Trapp, B. D., Shih, H. H., Farrer, R. G., Katz, D. A., et al. (1994). Childhood ataxia with diffuse central nervous system hypomyelination. *Annals of Neurology, 35*(3), 331–340.

Schoenfeld, R., Wong, A., Silva, J., Li, M., Itoh, A., Horiuchi, M., et al. (2010). Oligodendroglial differentiation induces mitochondrial genes and inhibition of mitochondrial function represses oligodendroglial differentiation. *Mitochondrion, 10*(2), 143–150.

Taanman, J. W. (1999). The mitochondrial genome: Structure, transcription, translation and replication. *Biochimica et Biophysica Acta, 1410*(2), 103–123.

Vafai, S. B., & Mootha, V. K. (2012). Mitochondrial disorders as windows into an ancient organelle. *Nature, 491*(7424), 374–383.

van der Knaap, M. S., Leegwater, P. A., Konst, A. A., Visser, A., Naidu, S., Oudejans, C. B., et al. (2002). Mutations in each of the five subunits of translation initiation factor eIF2B can cause leukoencephalopathy with vanishing white matter. *Annals of Neurology, 51*(2), 264–270.

van der Knaap, M. S., Pronk, J. C., & Scheper, G. C. (2006). Vanishing white matter disease. *The Lancet Neurology, 5*(5), 413–423.

van der Voorn, J. P., van Kollenburg, B., Bertrand, G., Van Haren, K., Scheper, G. C., Powers, J. M., et al. (2005). The unfolded protein response in vanishing white matter disease. *Journal of Neuropathology and Experimental Neurology, 64*(9), 770–775.

Van Haren, K., van der Voorn, J. P., Peterson, D. R., van der Knaap, M. S., & Powers, J. M. (2004). The life and death of oligodendrocytes in vanishing white matter disease. *Journal of Neuropathology and Experimental Neurology, 63*(6), 618–630.

Wong, K., Armstrong, R. C., Gyure, K. A., Morrison, A. L., Rodriguez, D., Matalon, R., et al. (2000). Foamy cells with oligodendroglial phenotype in childhood ataxia with diffuse central nervous system hypomyelination syndrome. *Acta Neuropathologica, 100*(6), 635–646.

Wong, Y. L., LeBon, L., Basso, A. M., Kohlhaas, K. L., Nikkel, A. L., Robb, H. M., et al. (2019). eIF2B activator prevents neurological defects caused by a chronic integrated stress response. *Elife*. https://doi.org/10.7554/elife.42940.